Check for updates

Received: 3 November 2023 | Revised: 15 February 2024 | Accepted: 8 April 2024

DOI: 10.1002/eqe.4130

RESEARCH ARTICLE

WILEY

Earthquake simulator testing of a three-story steel building for evaluating built-up box column performance and effect of sliding slab

Chung-Che Chou[1,2] | **Huang-Zuo Lin**[1] | **Alvaro Córdova**[1] | **Jian-Ming Chen**[1] | **Daniel Yen-Hsun Chou**[3] | **Shu-Hsien Chao**[2] | **Shih-Ho Chao**[4] | **Georgios Tsampras**[5] | **Chia-Ming Uang**[5] | **Hsin-Yang Chung**[3] | **Chin-Hsiung Loh**[1] | **Hsuan-Teh Hu**[3]

[1]Department of Civil Engineering, National Taiwan University, Taipei, Taiwan

[2]National Center for Research on Earthquake Engineering (NCREE), Taipei, Taiwan

[3]Department of Civil Engineering, National Cheng Kung University, Tainan, Taiwan

[4]Department of Civil Engineering, University of Texas, Texas, Arlington, USA

[5]Department of Structural Engineering, University of California, California, San Diego, USA

Correspondence
Chung-Che Chou, Department of Civil Engineering, National Taiwan University, Taiwan.
Email: cechou@ntu.edu.tw

Funding information
National Science and Technology Council

Abstract

The width-thickness requirement for highly ductile built-up box columns in AISC 341-22 is conservative when comparing the hysteretic responses of highly ductile box columns and I-shaped columns. This study aimed to assess the seismic performance of moderately ductile box columns in a 3-story steel dual frame with a buckling-restrained braced frame (BRBF) and a special moment frame (SMF). The frame specimen was configured in phase 1 testing to allow the slabs to slide relative to the steel frame; Teflon pads were provided between the slabs and steel beams, and horizontal buckling-restrained braces (BRBs) were installed between the slabs and steel beams. In phase 2, the horizontal BRBs were replaced by rigid links such that the frame specimen simulated a conventional construction. Two phases with 17 shake table tests were conducted on the frame specimen. A near-fault motion record, obtained from the 2022 Chihshang earthquake, was used as an input motion. In phase 1, test results showed that the slab sliding system was effective in reducing the floor acceleration by 25% when compared to the rigid slab frame system. In phase 2, the base of moderately ductile built-up box columns still performed well without local buckling even when the interstory drift angle reached 0.045 rad. Postearthquake tests were conducted on the all-steel, first-story BRB that was removed from the building specimen after all shake table tests. A higher-mode buckling of the core plate was observed at both ends of the core, causing a minor strength increase at the end of the test.

KEYWORDS
buckling restrained brace, built-up box column, shake table test, sliding slab

1 | INTRODUCTION

A steel dual system with a buckling-restrained braced frame (BRBF) and a special moment frame (SMF) is expected to perform well in earthquakes when inelastic action can occur in the braces, beam ends, and column bases. The first-story columns under high axial load and flexural moment may develop local buckling near the column base and cause strength

 © 2024 John Wiley & Sons Ltd.

degradation. The requirement for the width–thickness ratio (b/t) of built-up box columns in AISC 341-22[1] is the same as that in AISC 341-16.[2] The column section requirement in a BRBF has been tightened from being moderately ductile to highly ductile if the column is expected to experience significant plastic deformation in a large earthquake. However, the highly ductile built-up box column can perform very well without showing strength degradation even at high axial load and high lateral drift when compared to that of the I-shaped deep columns that show significant strength degradation under the same loading condition.[3,4] The performance difference indicates that the b/t requirement for the highly ductile built-up box column in AISC 341-22 may be overly conservative and may be relaxed.

Cyclic behavior of isolated columns with highly ductile or moderately ductile built-up box members was the focus of recent research.[3–6] To simulate the rotating effect at the top end of the first-story columns, some tests were conducted on steel columns with rotation flexibility at the column top end or using a subassemblage frame with beams and upper-story columns to simulate a more realistic boundary condition at the column top end.[7–11] However, very limited shake table tests at the system level have been conducted to study the seismic response of first-story columns, especially those with moderately ductile built-up box columns. To date, only a full-scale shake table collapse test of a four-story steel SMF with hollow structural section (HSS) columns was conducted at the E-Defense facility in Japan.[12,13] The collapse test showed a side-sway first-story collapse mechanism, but the b/t ratio of the HSS column was 31.3, exceeding the design limit for moderately ductile box columns in AISC 341-16 and AISC 341-22.

The research reported in this paper also explores the potential of a new steel building frame system with sliding slabs for controlled force transferred from the slab to the steel frame. Traditionally, the slab is rigidly connected to the lateral force-resisting system (LFRS) in a steel frame using shear studs. Various solutions have been explored to mitigate the seismic demand in buildings by using story isolation. For example, Mar and Tipping[14] presented structural details for a story isolation system that reduces the base shear and roof acceleration demand. Villaverde[15,16] proposed the use of a roof isolation system that consists of flexible laminated rubber bearings between a building's roof and the columns, and viscous dampers between the roof and the rest of the building. Numerical simulation of a building model showed reduction in the roof drift. Villaverde et al.[17] further conducted a small-scale shake table test to assess the response of a building model with and without the roof isolation system, verifying that a reduction in the seismic responses could be achieved when the roof isolation was used. Cui et al.[18,19] studied the seismic response of a bidirectional spring unit in seismically isolated floors through component-level and system-level experimental testing. Liu and Warn[20] studied the sensitivity of the response of seismic isolated floor systems in multistory steel shear wall structures. Anajafi and Medina[21] assessed the effect of various parameters affecting the design of multifloor isolation systems. Casagrande et al.[22] assessed the use several types of dampers to isolate selected floor systems in buildings. Xiang et al.[23,24] introduced a floor-isolation system for steel frames that use laminated visco-elastic material to connect the floor to the steel beam.

To further study the seismic performance of built-up box columns in a BRBF, shake table tests were conducted on a full-scale, three-story steel dual frame system with moderately ductile built-up box members per AISC 341-22; all-steel sandwiched buckling-restrained braces (SBRBs) were used in the BRBF.[25] The research objective is two-fold. The first objective is to evaluate the system performance of the floor-isolated building. In addition to the diagonal SBRB, which is called D-SBRB and is intended to remain elastic, horizontal SBRBs (H-SBRBs) were used between the vertical steel frame and the Teflon-isolated slabs to dissipate energy. The test building was then modified for the objective of evaluating the effect of the width-thickness ratio of built-up box columns at the system level. The modification included replacing the H-SBRBs by "rigid" members to simulate the conventional construction with the slabs rigidly connected to the steel frame. D-SBRB served as the energy dissipated elements which also imposed high axial load to the columns in this phase of testing.

2 | STEEL DUAL FRAME SPECIMEN

The specimen was a full-scale, three-story steel building with precast concrete slabs. It was designed for a site classified as a stiff soil and was located 3.5 km from the Xinhua fault in Tainan, Taiwan. Figure 1A and B show the plan and elevation views, with the LFRS along column line B positioned in the shaking direction (north-south direction). The LFRS was a two-dimensional, two-bay dual system that consisted of an SMF and a BRBF. The gravity force-resisting system (GFRS), not designed to provide lateral load resistance, was positioned at the perimeter of the building. The LFRS was designed with an SMF in the north bay and a BRBF in the south bay. The total height of the specimen was 9000 mm. Two concrete blocks, labeled as "CB" in the figure, were placed on each floor, resulting in a weight of 59 kN for the bottom two floors and 74 kN for the roof. The total weight was 333 kN for the bottom two floors and 335 kN for the roof. According to

10969845, 2024, 9, Downloaded from https://onlinelibrary.wiley.com/doi/10.1002/eqe.4130 by Georgios Tsampras - University Of California , Wiley Online Library on [07/11/2026]. See the Terms and Conditions (https://onlinelibrary.wiley.com/terms-and-conditions) on Wiley Online Library for rules of use; OA articles are governed by the applicable Creative Commons License

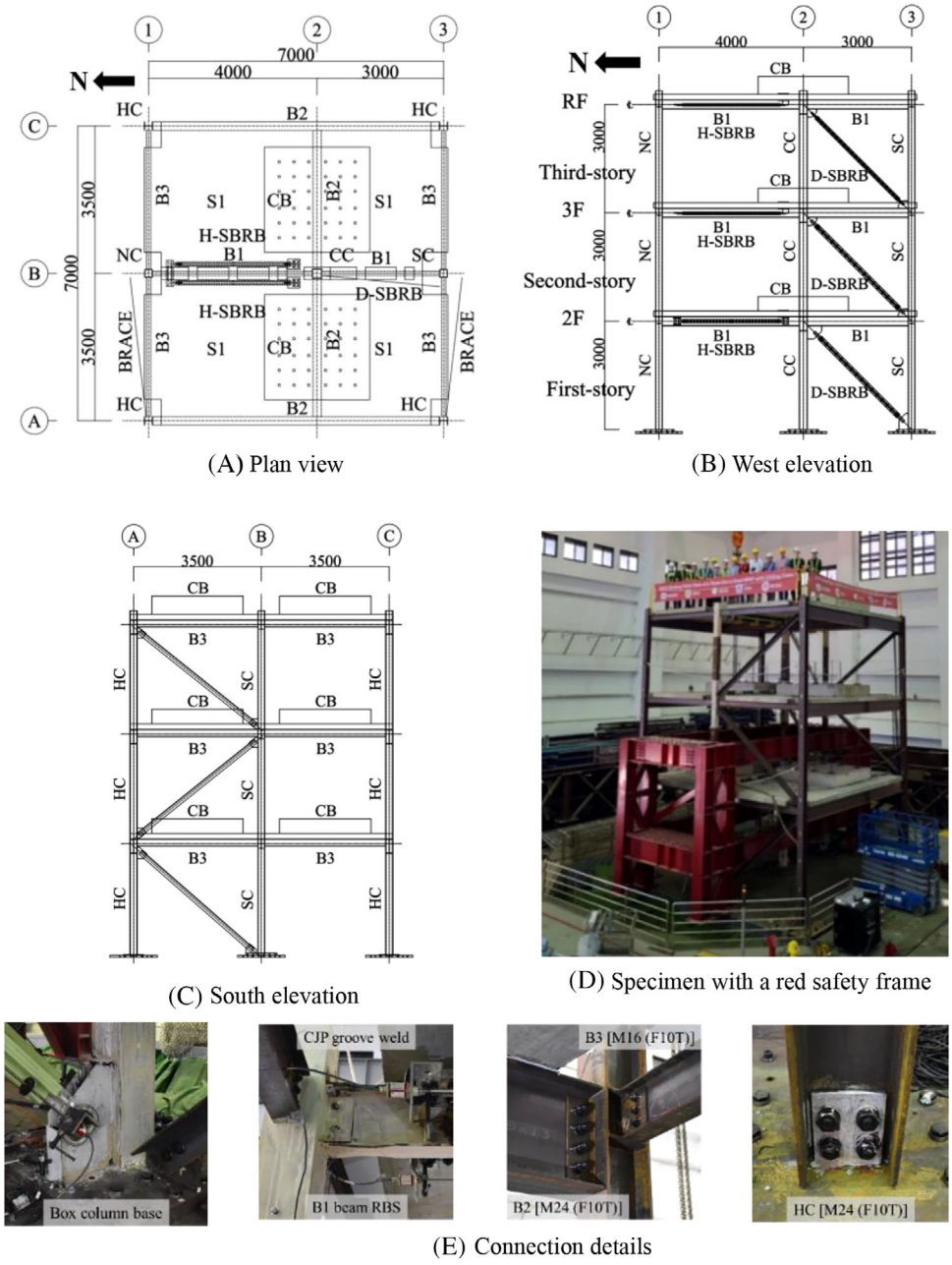


FIGURE 1 Test specimen (unit: mm).

Taiwan Seismic Building Code,[26] the empirical structural period used for calculating the design base shear was 0.26 s. The seismic design base shear, derived from the site spectrum (Figure 2A), was 0.242 W (=238 kN) with W representing the total building weight.

2.1 | Lateral force-resisting system (LFRS)

Table 1 lists the column and beam sections. SN490B steel, with a nominal yield stress of $F_y = 325$ MPa, was specified for all square built-up box columns, wide-flange columns, built-up I-shaped beams, and SBRBs. The measured steel mechanical properties, including the yield stress, F_{ym}, and ultimate stress, F_{um}, are summarized in Table 2. The north column (NC), center column (CC), and south column (SC) had flange width–thickness ratios (b/t) of 21.1, 20.5, and 21.1, respectively.

10969845, 2024, 9, Downloaded from https://onlinelibrary.wiley.com/doi/10.1002/eqe.4130 by Georgios Tsampras - University Of California , Wiley Online Library on [07/11/2026]. See the Terms and Conditions (https://onlinelibrary.wiley.com/terms-and-conditions) on Wiley Online Library for rules of use; OA articles are governed by the applicable Creative Commons License

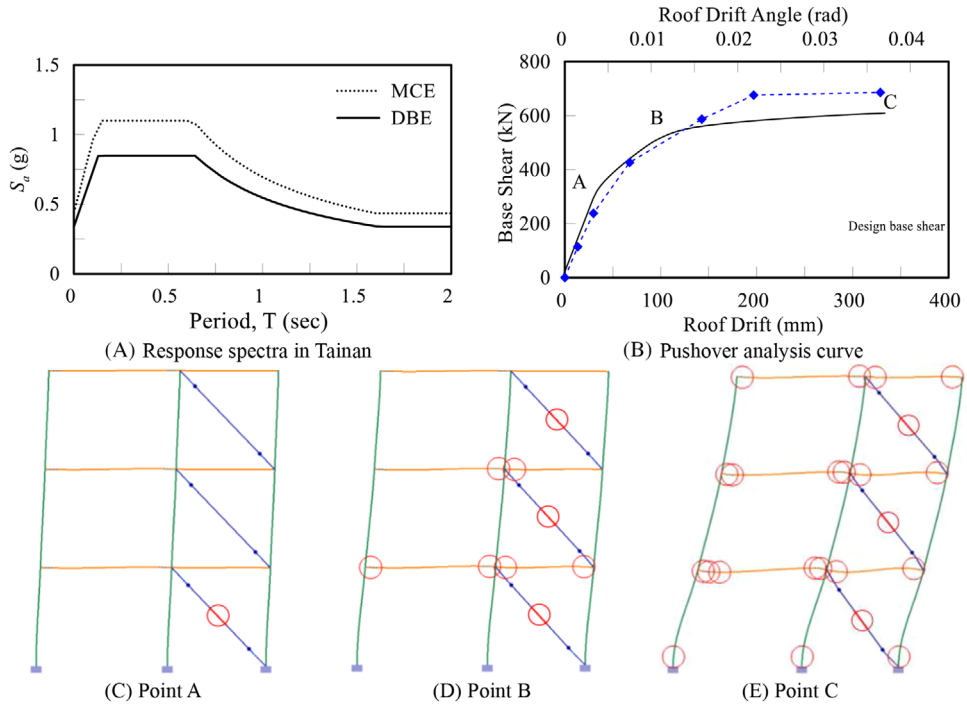


FIGURE 2 Design response spectra and pushover analysis results.

TABLE 1 Column and beam sections.

Element	Location		Section (mm)
Column	LFRS (1st–3rd story)	North	NC: Box 185 × 185 × 8
		Center	CC: Box 225 × 225 × 10
		South	SC: Box 185 × 185 × 8
	GFRS (1st–3rd story)		HC: H 200 × 200 × 8 × 12
Beam	LFRS (2F–RF)		B1: H 257 × 102 × 6 × 9
	GFRS (2F–RF)		B2: H 400 × 200 × 8 × 13
			B3: H 200 × 100 × 5.5 × 8

CC, center column; LFRS, lateral force-resisting system; NC, north column; SC, south column.

These b/t values met the moderately ductile column requirement (λ_{md}), but not the highly ductile requirement (λ_{hd}) in AISC 341-22[1]:

$$\lambda_{hd} = 0.55\sqrt{\frac{E}{R_y F_y}} \tag{1}$$

$$\lambda_{md} = 1.0\sqrt{\frac{E}{R_y F_y}} \tag{2}$$

By using $E = 200$ GPa, $F_y = 325$ MPa, and $R_y = 1.25$, the λ_{hd} and λ_{md} values for the flange plates equal 12.2 and 22.2, respectively. The column base was bolted to the shake table as a fixed end. The first-story CC carried an axial gravity load of $0.1P_y$, while the SC and NC carried axial gravity loads of $0.03P_y$ and $0.04P_y$, respectively. Built-up I-shaped beams (H257 mm × 102 mm × 6 mm × 9 mm) with a reduced beam section (RBS) near the moment connection (Figure 1E) were used for the SMF. Beam flanges and web were connected to the column flange using CJP groove welds. The steel backing at the beam top flange was not removed, and an 8-mm fillet weld was added between the steel backing and the column flange. However, the steel backing between the bottom flange of the beam and column was removed, and the root pass was back gouged to sound weld metal before being back welded with an 8-mm reinforcing fillet.[27] No RBS was used in the BRBF

10969845, 2024, 9, Downloaded from https://onlinelibrary.wiley.com/doi/10.1002/eqe.4130 by Georgios Tsampras - University Of California , Wiley Online Library on [07/11/2026]. See the Terms and Conditions (https://onlinelibrary.wiley.com/terms-and-conditions) on Wiley Online Library for rules of use; OA articles are governed by the applicable Creative Commons License

TABLE 2 Measured steel properties from coupon tests.

Coupon	Thickness (mm)	F_y (MPa)	F_u (MPa)	Average F_y (MPa)	Average F_u (MPa)	$\frac{F_u}{F_y}$	R_y
8-1	8	399	550	399	550	1.38	1.23
8-2		399	550				
9-1	9	410	559	411	559	1.36	1.26
9-2		412	559				
10-1	10	410	571	415	571	1.38	1.28
10-2		419	571				
12-1	12	383	496	383	495	1.29	1.18
12-2		383	494				

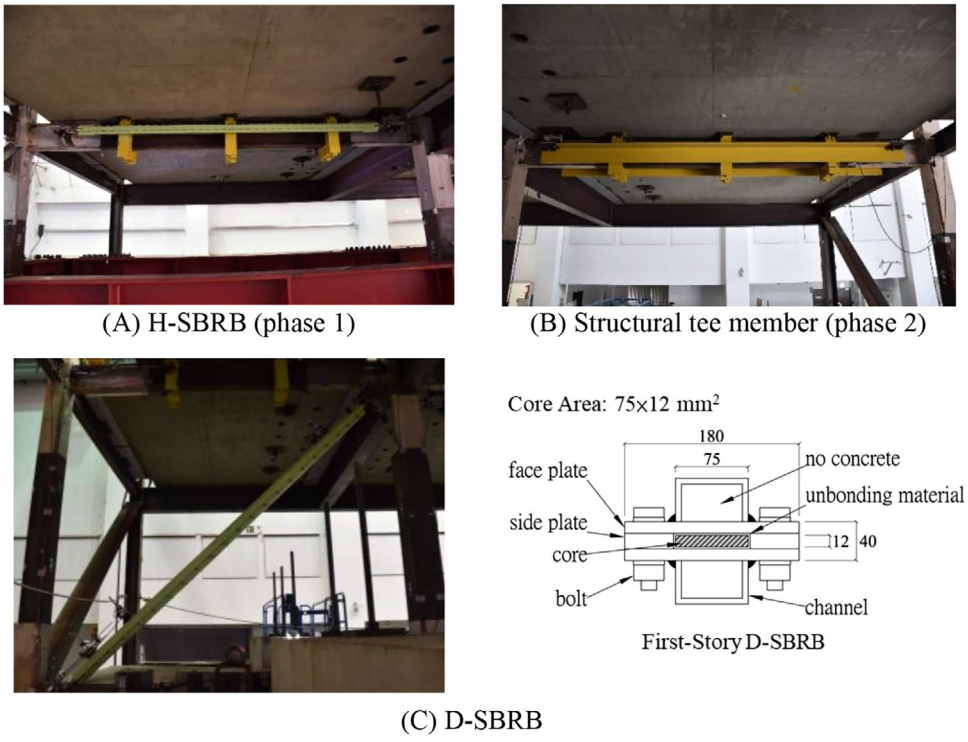


FIGURE 3 Beam lateral bracing and all-steel sandwiched buckling-restrained brace (SBRB).

bay. The beams met the highly ductile member requirements; lateral bracing was provided 1 m on center along the beam span (see yellow brackets in Figure 3).

A type of steel-only SBRB was used in the BRBF bay for lateral earthquake resistance. The SBRB consisted of a steel core and a pair of bolted restraining members, with no concrete filled in the restraining member, as shown in Figure 3C. The SBRBs were designed following the procedure described in Chou and Chen.[28] The SBRBs in the first and second stories had a core plate of 75 × 12 mm, a pair of channel of 75 × 45 × 6 mm, and a pair of face plate of 180 × 12 mm. In the third story, the SBRBs had a core plate of 50 × 8 mm, channels of 50 × 35 × 6 mm, and face plates of 155 × 12 mm. The ratios between the Euler buckling force of the restraining member and the core yield force ranged from 3.2 to 3.5, exceeding the design recommendation of 2.5.[28] All SBRBs were connected to the frame by using a dual-gusset-plate configuration.[29,30] The weak axis of the SBRB core was oriented transversely to the dual-gusset-plate connection, which excluded the weak-axis buckling of the SBRBs due to the significantly large in-plane rotational stiffness at the BRB-to-gusset end.

10969845, 2024, 9, Downloaded from https://onlinelibrary.wiley.com/doi/10.1002/eqe.4130 by Georgios Tsampras - University Of California , Wiley Online Library on [07/11/2026]. See the Terms and Conditions (https://onlinelibrary.wiley.com/terms-and-conditions) on Wiley Online Library for rules of use; OA articles are governed by the applicable Creative Commons License

2.2 | Gravity force-resisting system (GFRS)

The GFRS along column Lines A and C in Figure 1A consists of wide-flange columns (HC) at the corners and beams (B2 and B3). All gravity beams were connected to the columns with simple framing (i.e., shear plate and bolts) as shown in Figure 1E. For B2 gravity beams, a 110 × 325 × 9 shear tab and four M24 (F10T) bolts were used, while for B3 gravity beams, a 110 × 160 × 9 shear tab and three M16 (F10T) bolts were used. The gravity columns (HC) were also pinned at the base by using a 165 × 180 × 15 plate and four M24 (F10T) bolts, as shown in Figure 1E. To increase the lateral stiffness of the building transverse to the shaking direction, diagonal braces were installed in the east–west direction as shown in Figure 1C.

2.3 | Test phase

The shake table test was conducted in two phases. In phase 1, two H-SBRBs were installed beneath each floor to provide energy dissipation when the slab moves relative to the supporting beams (Figures 1B and 3A). One end of each H-SBRB was connected to the slab and the other end was connected to a steel beam. Teflon pads were placed between the precast slab and the beams to minimize friction. Since no shear studs were used between the beam and the slab, the slab was allowed to slide, thereby transferring the inertial force from the floor to the steel frame via these H-SBRBs. In phase 2, all H-SBRBs were replaced by structural tee members with high axial stiffness and strength to simulate a rigid connection between the slab and beam (Figure 3B). The test specimen was heavily instrumented, which included 262 strain gauges, 47 displacement transducers, 28 accelerometers, and 16 linear variable differential transducers (LVDTs). A motion-capture system with 221 sensors was also used to record the slab, frame, and SBRB responses.

2.4 | Nonlinear pushover analysis

A nonlinear static pushover analysis was conducted on the frame specimen using the PISA3D computer program.[31] Beam and column members were modeled using a beam-column element with nonlinear parameters and a lumped plasticity approach; the beam-to-column joint included a rigid end zone. The D-SBRB was modeled using a truss element with isotropic and kinematic hardening material parameters based on Chou et al.[29] Figure 2B shows the pushover analysis response of the specimen. The first yield of the specimen (Point A) occurs in the first-story D-SBRB (Figure 2C). The force level is close to the design base shear, consistent with the frame design. As the frame is deformed to 0.012 rad roof drift (Point B), all braces as well as the second and third floor beams form plastic hinges (Figure 2D). Finally, the column base and other beam yielding occur beyond 0.03 rad at Point C (Figure 2E).

3 | H-SBRB DESIGN PROCEDURE

Figure 4 shows the mechanism of slab sliding, where $\Delta_{s,x}$ is the slab displacement, $\Delta_{f,x}$ is the frame displacement, and $\delta_{H,x}$ is the H-SBRB axial deformation. Ignoring the diaphragm and beam axial deformation, the lateral displacement of the slab is the summation of the frame lateral displacement and the H-SBRB deformation:

$$\Delta_{s,x} = \Delta_{f,x} + \delta_{H,x} \tag{3}$$

When the concrete slab is rigidly connected to the steel beams as in conventional construction, the design diaphragm force, F_{px}, at the Design Base Earthquake (DBE) level can be determined based on section 12.10.1 in ASCE 7-22,[32] as listed in Table 3. In phase 2 when the sliding slab was "locked" by the structural tee members to mimic the rigidly connected slab, the required seismic overstrength forces that needed to be transferred through these members were computed as the F_{px} forces multiplied by 3.75, which is 1.5 times the system overstrength factor, Ω_0 (=2.5 for a dual system with a BRBF). The design force is high because the frame specimen is expected to test to a ground motion level that is much larger than the Maximum Considered Earthquake (MCE) level. In phase 1 with the slabs allowed to slide with respect to the steel frame, ASCE 7-22 does not provide any guidelines. To promote sliding such that energy dissipation can occur in the H-SBRB devices, it was judged through preliminary nonlinear time history analyses that multiplying the F_{px} forces by 1.5, which

10969845, 2024, 9, Downloaded from https://onlinelibrary.wiley.com/doi/10.1002/eqe.4130 by Georgios Tsampras - University Of California , Wiley Online Library on [07/11/2026]. See the Terms and Conditions (https://onlinelibrary.wiley.com/terms-and-conditions) on Wiley Online Library for rules of use; OA articles are governed by the applicable Creative Commons License

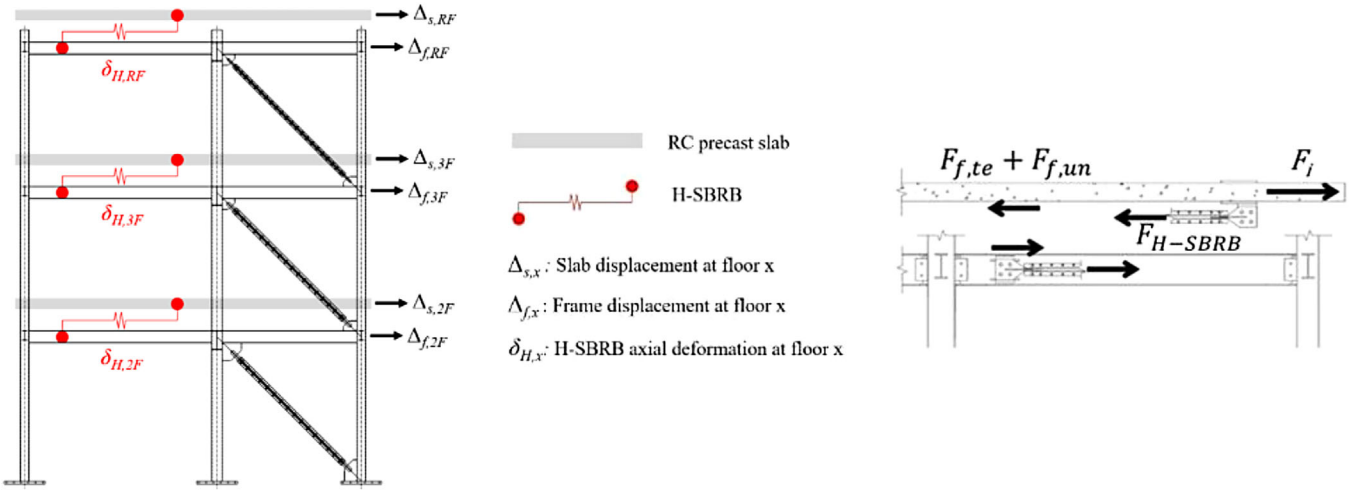


FIGURE 4 Sliding slab mechanism.

TABLE 3 Design force for horizontal sandwiched buckling-restrained brace (H-SBRB) and tee member.

Floor	F_x (kN)	F_{px} (kN)	H-SBRB force (kN)	WT member force (kN)
Roof	119	110	165	413
Third	79	98	147	368
Second	40	79	119	296

is smaller than Ω_0, was reasonable. Therefore, required forces (see Table 3) were used to size H-SBRBs and structural tee members.

4 | GROUND MOTION FOR SHAKE TABLE TEST

The unidirectional shake table test was conducted at the NCREE Tainan laboratory. The size of the shaking table is 8 m by 8 m with a payload capacity of 2000 kN. The selected ground motion was obtained from the September 18th, 2022, Chihshang earthquake, recorded at the EYUL-EW station close to a collapsed three-story building.[33] The recorded acceleration time history was baseline-corrected by following the method described in Iwan et al.[34] Then, it was high-pass filtered to remove the residual displacement (Figure 5A). The response spectrum of the input motion without any scaling is close to the design response spectrum at the DBE level. Figure 5B and C show the response spectra for the tests conducted in each phase, where each spectrum was computed from the measured shake table motion. The peak pulse period at time around 11 s (Figure 5A) is about 0.5 s, which is close to specimen's first mode period ($T_n = 0.52$ s).

Seven tests were conducted in phase 1. The test started at a peak ground acceleration (PGA) of 0.032 g in test 1, which corresponded to about 5% of the DBE intensity, and gradually increased to 0.62 g in test 7. In phase 2, 10 tests were conducted on the frame specimen, starting with a similar intensity as in phase 1 and reaching 1.05 g in test 10. Table 4 lists all motion intensities in phase 1 and 2 tests. A white noise test with an intensity of 0.015 g was conducted on the specimen after each test to obtain the structural period. The identified first mode period is also listed in Table 4. Figure 5B and C show the response spectra together with the design spectra at DBE level and MCE level, where PGA = 0.44 g for the latter. By examining the response spectra at $T = 0.52$ s, the motion intensity in test 5 approximates the DBE level, and the test 6 approximates the 1.2 × MCE level. The motion intensities in tests 7 and 10 are about 1.4 and 2.4 (=1.05/0.44) times the MCE level, computed based on their respective PGA and the design PGA of 0.44 g. The story force was determined from the inertia forces of both the slabs and steel frame by multiplying the measured accelerations and masses of the slab and steel frame, respectively, at each floor. The slab acceleration at each floor was obtained by four accelerometers evenly placed on the slab, while the frame acceleration was recorded by accelerometers positioned at the beam-to-box column panel zone at each floor.

10969945, 2024, 9, Downloaded from https://onlinelibrary.wiley.com/doi/10.1002/eqe.4130 by Georgios Tsampras - University Of California , Wiley Online Library on [07/11/2026]. See the Terms and Conditions (https://onlinelibrary.wiley.com/terms-and-conditions) on Wiley Online Library for rules of use; OA articles are governed by the applicable Creative Commons License

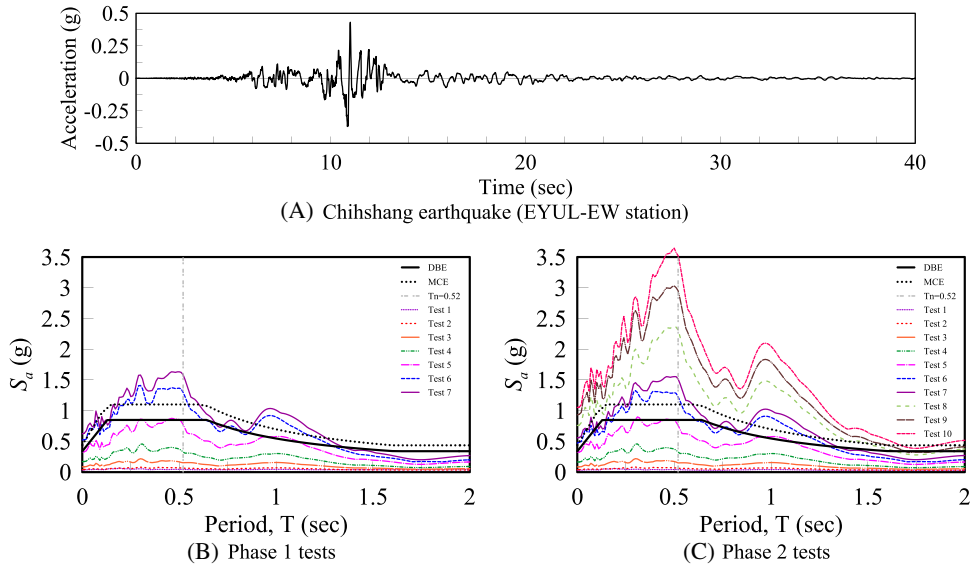


FIGURE 5 Earthquake motion and response spectra.

TABLE 4 Maximum roof drift in phases 1 and 2.

Test no.	PGA (g)	Peak roof drift (mm) [drift angle ($\times 10^{-2}$ rad)]	Residual roof drift (mm) [drift angle ($\times 10^{-2}$ rad)]	Period (s)
(a) Phase 1				
1	0.032	3 (0.03)	0 (0)	0.52
2	0.039	4 (0.05)	0 (0)	0.48
3	0.085	14 (0.15)	0 (0)	0.49
4	0.17	29 (0.32)	−1 (−0.01)	0.49
5	0.33	61 (0.68)	−2 (−0.02)	0.57
6	−0.52	−117 (−1.3)	−28 (−0.31)	0.54
7	0.62	141 (1.56)	3 (0.03)	0.49
(b) Phase 2				
1	0.028	0 (0)	3 (0.03)	0.52
2	0.038	2 (0.02)	3 (0.03)	0.55
3	0.083	13 (0.15)	3 (0.03)	0.48
4	0.16	30 (0.33)	2 (0.02)	0.60
5	0.33	68 (0.75)	−0.2 (0)	0.62
6	−0.47	−116 (−1.29)	−19 (−0.21)	0.61
7	0.56	143 (1.59)	6 (0.07)	0.58
8	0.76	197 (2.19)	47 (0.52)	0.53
9	−0.93	−290 (−3.22)	−69 (−0.77)	0.57
10	1.05	329 (3.65)	65 (0.72)	0.54

PGA, peak ground acceleration.

5 | OVERALL FRAME RESPONSE IN TESTS

Figure 6A and B show the roof drift history in phases 1 and 2. In phase 1, the sign of the input motion was reversed for test 6 after the specimen completed test 5 at the DBE level with a residual roof drift of −0.00011 rad. The frame's maximum roof drift angle was −0.013 rad, with a residual drift of −0.0031 rad in test 6. In test 7 (1.4 × MCE level), the original motion was reapplied to the specimen to limit the residual drift. This resulted in a maximum roof drift angle of 0.0156 rad with a very

10969845, 2024, 9, Downloaded from https://onlinelibrary.wiley.com/doi/10.1002/eqe.4130 by Georgios Tsampras - University Of California , Wiley Online Library on [07/11/2026]. See the Terms and Conditions (https://onlinelibrary.wiley.com/terms-and-conditions) on Wiley Online Library for rules of use; OA articles are governed by the applicable Creative Commons License

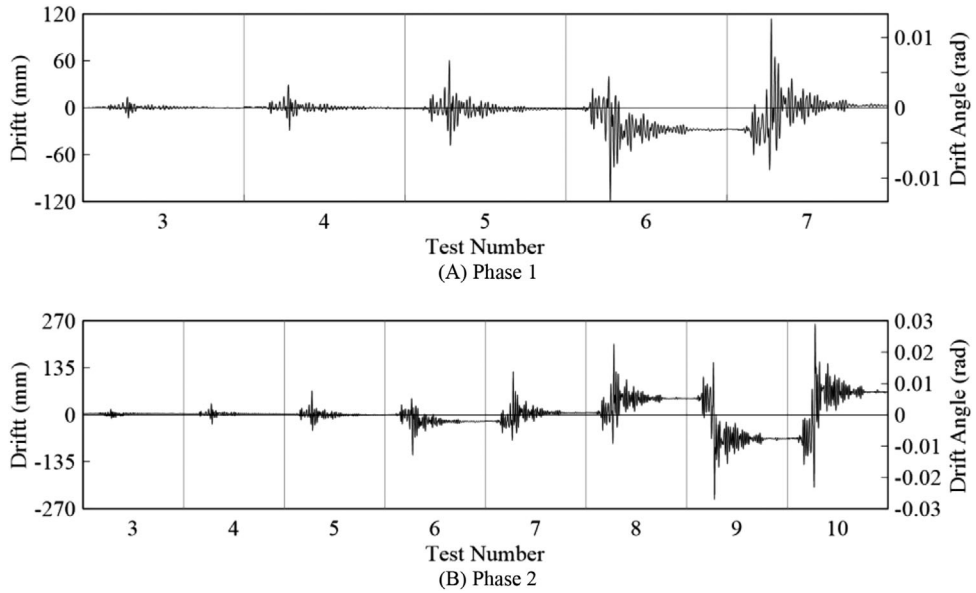


FIGURE 6 Roof drift response.

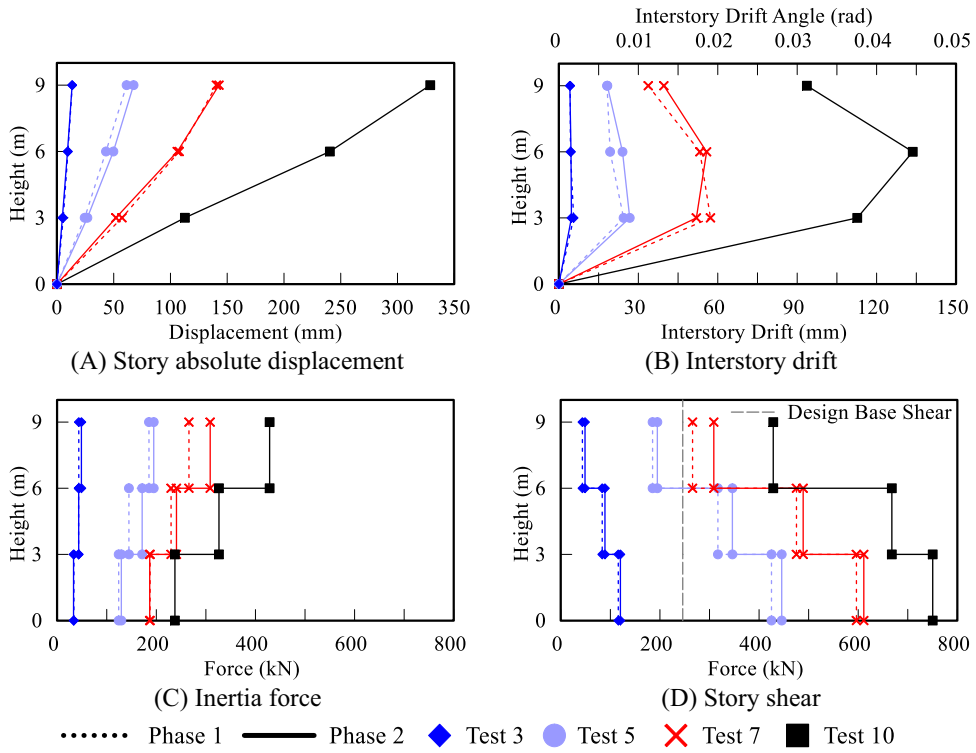


FIGURE 7 Maximum story shears and drifts.

small residual drift (Figure 6A), which facilitated the disassembly of the H-SBRBs from the specimen and the installation of structural tee members for phase 2 tests.

For comparison purposes, the frame specimen in phase 2 underwent the same motion and test sequence as in phase 1. Tests 6 and 7 in phase 2 showed slightly lower maximum accelerations compared to those in phase 1 (see Table 4). Figure 7A shows the displacement profiles in tests 3, 5, 7, and 10 in both test phases, with a maximum roof drift, $\Delta_u = 329$ mm, in test 10. The maximum interstory drift angle of the specimen was 0.045 rad in the second story, as shown in Figure 7B. Figure 7C and D show the peak story force and shear during tests 3, 5, 7, and 10 in both test phases. The story force in the

10969845, 2024, 9, Downloaded from https://onlinelibrary.wiley.com/doi/10.1002/eqe.4130 by Georgios Tsampras - University Of California , Wiley Online Library on [07/11/2026]. See the Terms and Conditions (https://onlinelibrary.wiley.com/terms-and-conditions) on Wiley Online Library for rules of use; OA articles are governed by the applicable Creative Commons License

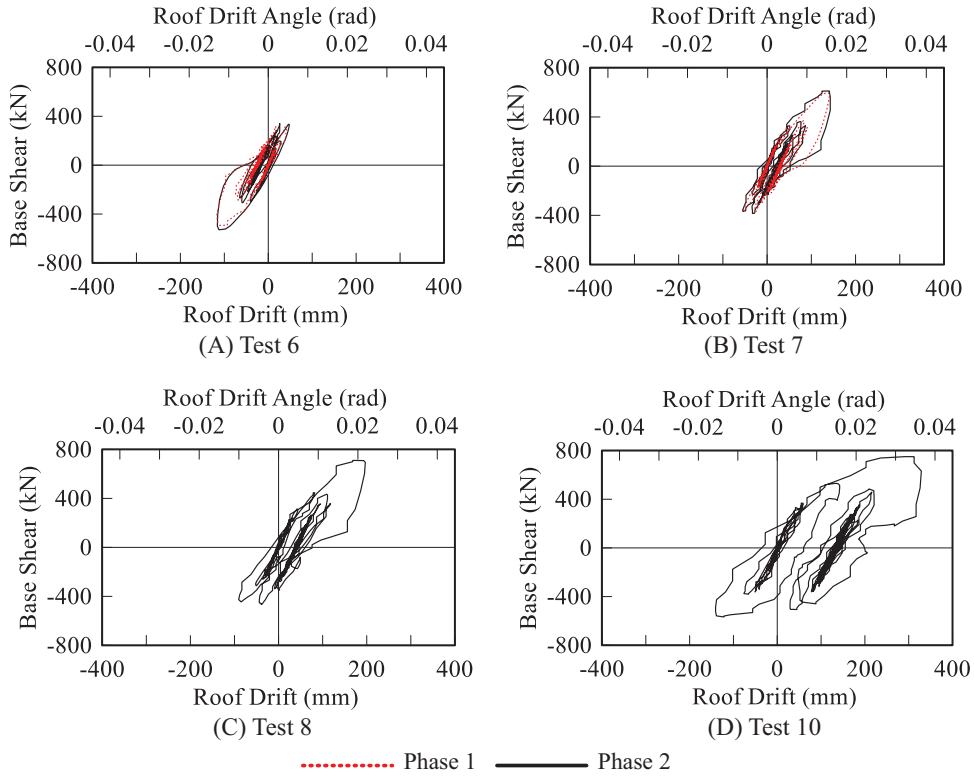


FIGURE 8 Base shear versus roof drift.

top story has a significant difference between the two phases, with phase 1 being 15% less than phase 2. The differences in the bottom two stories were not significant (i.e., 3% difference) because the acceleration response tends to be greater at the roof. When comparing the responses between two phases, it should be pointed out that the measured PGA values were about 11% larger in phase 1 tests, although the controlling parameters for the table input motion were the same in the tests. The tests indicated the effectiveness of slab sliding in reducing the floor acceleration. Figure 8 shows the overall response during tests 6, 7, 8, and 10, where no strength degradation was observed even under the strongest motion intensity with PGA = 1.05 g in test 10. The overall responses in phase 1 and 2 tests are similar because the input motion intensities are similar, as shown in Figure 2B, which plots the base shear versus the roof drift. The change in the specimen's lateral stiffness starts around the level of the design base shear, close to the test 4. Note that the base shear increase in test 10 is not significant compared to the previous tests due to column yielding. The maximum base shear is 750 kN, about 3.2 times the design base shear of 238 kN. If the ideal yield displacement of the frame specimen is $\Delta_y = 85$ mm (see Figure 2B), the system ductility factor is 3.9 (=329/85) in test 10.

5.1 | Slab response

Slab sliding causes a relative movement between the slab and the LFRS, which represents the H-SBRB axial deformation (Figure 4). Slab sliding was first observed in test 4 of phase 1 at PGA = 0.17 g and the sliding displacement increased with the magnitude of the motion. Figure 9 shows the H-SBRB deformation at each floor in test 7 of phase 1. The largest deformation (=11 mm) was observed at the roof, while the second floor had the lowest H-SBRB deformation (3 mm). Figure 10A shows that the relative displacement measured during test 7 in phase 1 is significantly larger than that in phase 2, where the structural tee member was used to simulate a nearly rigid connection between the slab and the frame. Figure 11A and B show the hysteretic response of the structural tee member and H-SBRB at the roof. Energy dissipation is evident in the H-SBRB but not in the structural tee member during test 7.

Ideally, the relative displacement between the slab and the frame should equal the H-SBRB axial deformation [$\delta_{H,x}$ in Equation 3]. However, a 3 mm difference was observed between the maximum relative displacement [i.e., 14 mm in Figure 10A] and the maximum axial displacement of H-SBRB [i.e., 11 mm in Figure 9C]. The difference was caused by the

10969945, 2024, 9, Downloaded from https://onlinelibrary.wiley.com/doi/10.1002/eqe.4130 by Georgios Tsampras - University Of California , Wiley Online Library on [07/11/2026]. See the Terms and Conditions (https://onlinelibrary.wiley.com/terms-and-conditions) on Wiley Online Library for rules of use; OA articles are governed by the applicable Creative Commons License

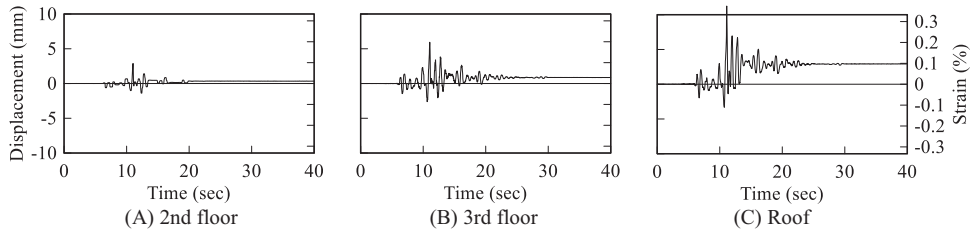


FIGURE 9 Horizontal sandwiched buckling-restrained brace (H-SBRB) axial deformation in test 7 (phase 1).

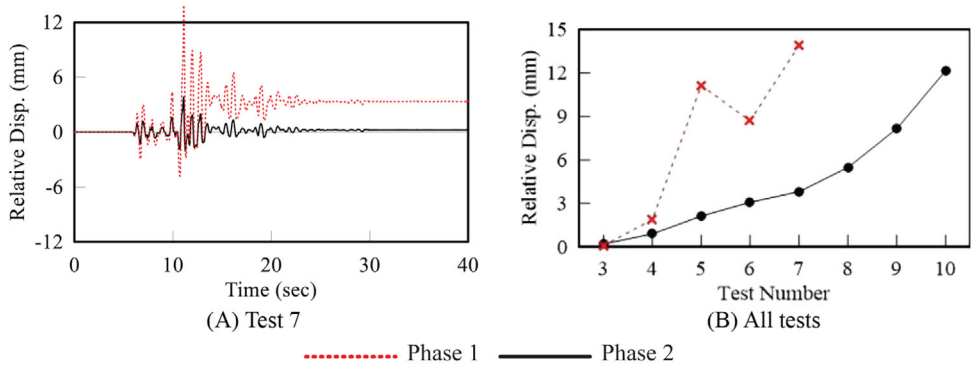


FIGURE 10 Roof relative displacement between the slab and frame in phases 1 and 2.

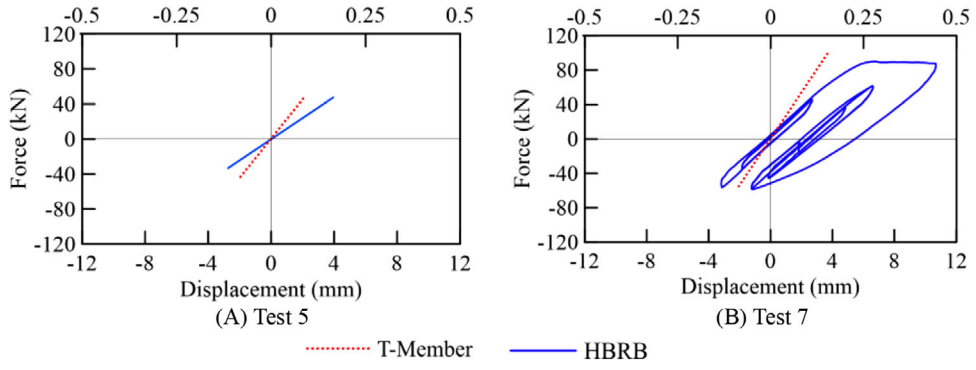


FIGURE 11 Structural tee member and horizontal sandwiched buckling-restrained brace (H-SBRB) response at the roof level (phases 1 and 2).

connection flexibility at H-SBRB ends, which has a load eccentricity of 100 mm between the floor-to-gusset connection and the H-SBRB centerline axis. For H-SBRB to be more effective, testing showed that the end flexibility should be minimized.

Figure 12 shows the floor absolute accelerations measured directly from accelerometers positioned on the frame (at the panel zone) and the slab. A comparison between the frame and slab accelerations shows a noticeable reduction in the peak acceleration on the roof in test 7 (Figure 12A). Figure 12B shows the absolute acceleration at each floor during the tests. The difference between phases 1 and 2 starts from test 5 and is significant in test 7. Figure 12C shows the slab acceleration profiles normalized by the shake table peak acceleration. It shows a significant reduction in slab acceleration at all floors in phase 1, with a 25% reduction at the roof, even though phase 1 test had a larger PGA compared to phase 2 test (0.62 vs. 0.56 g in Table 4). This reduction in slab acceleration also resulted in a decrease in story shear, as shown in Figure 7C and D. Moreover, Figure 12D shows that the ratio of the slab to frame acceleration in phase 2 is close to a unity up to test 8 (i.e., 1.7 × MCE level), indicating minimal slab sliding and similar accelerations in both the frame and slab.

10969845, 2024, 9, Downloaded from https://onlinelibrary.wiley.com/doi/10.1002/eqe.4130 by Georgios Tsampras - University Of California , Wiley Online Library on [07/11/2026]. See the Terms and Conditions (https://onlinelibrary.wiley.com/terms-and-conditions) on Wiley Online Library for rules of use; OA articles are governed by the applicable Creative Commons License

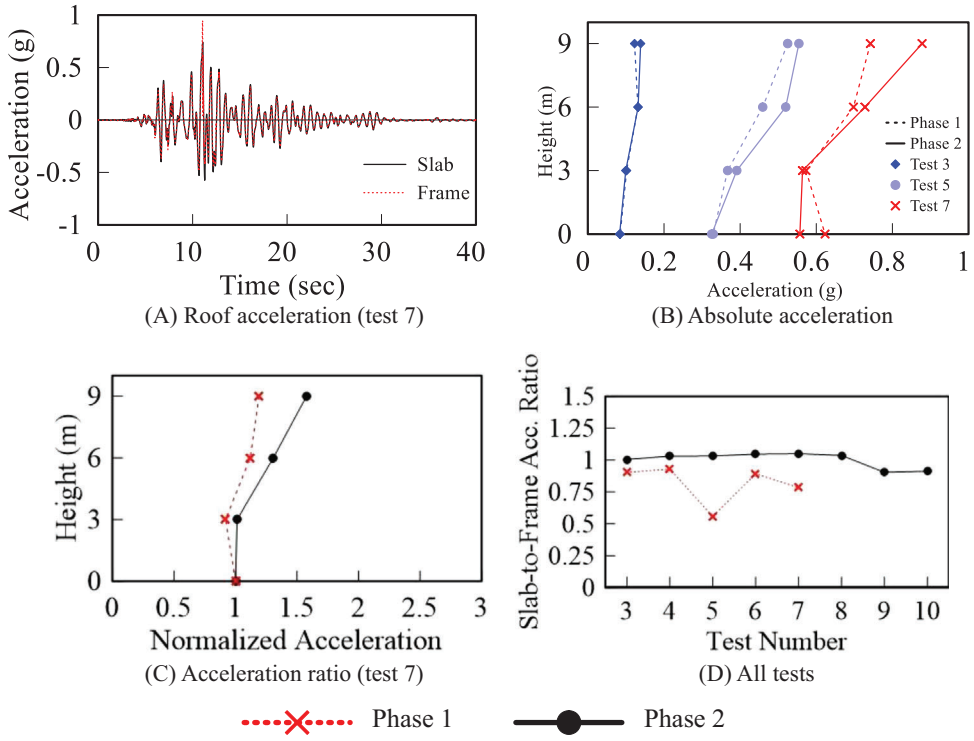


FIGURE 12 Floor accelerations.

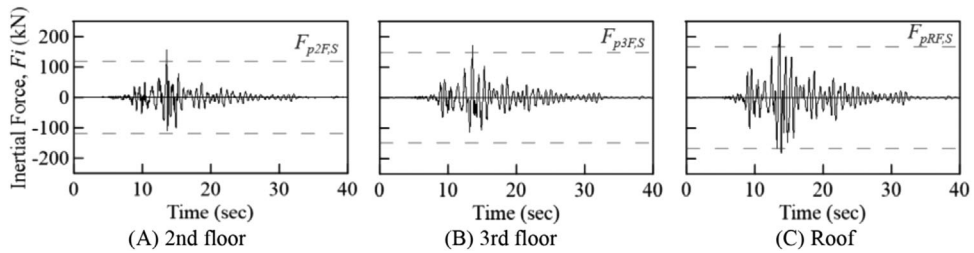


FIGURE 13 Inertial forces in test 6 (phase 1).

5.2 | H-SBRB response

This section aims to evaluate the force of the horizontal energy dissipation device (i.e., H-SBRB) and its effect on the floor response in the tests. The test 6 data is more representative than other tests for this purpose because the motion intensity of test 6 is close to the MCE level, which is close to the H-SBRB design force. Figure 13 shows that the H-SBRB design forces at three floors ($F_{p2F,S}$ $F_{p3F,S}$ $F_{pRF,S}$) in Table 3 were reached or slightly exceeded. By multiplying the peak floor acceleration and floor mass to obtain the inertial force at each floor (Figure 14B and C), the inertial forces at the second floor and roof were close to the design values, which were amplified by a factor of 1.2 and 1.4 to obtain a similar shaking force in tests 6 (1.2 × MCE level) and 7 (1.4 × MCE level).

Figure 4 shows a schematic diagram for the slab force equilibrium:

$$F_{f,un} = F_i - F_{f,te} - F_{\text{H-SBRB}} \tag{4}$$

where F_i is the inertial force, $F_{f,te}$ is the friction force, $F_{\text{H-SBRB}}$ is the axial force of the H-SBRB, and $F_{f,un}$ is the unintended friction force. The friction coefficient of the Teflon pad was 6.3%, which was obtained from a one-story subassemblage test.[35] The unintended force observed in tests was mainly caused by friction between the beam flange and its lateral bracing in the LFRS used to prevent the out-of-plane movement of the beam (see the yellow bracket in Figure 3). The other possible source was the friction force between the slab and the side plate on the beam top flange in the GFRS to

10969945, 2024, 9, Downloaded from https://onlinelibrary.wiley.com/doi/10.1002/eqe.4130 by Georgios Tsampras - University Of California , Wiley Online Library on [07/11/2026]. See the Terms and Conditions (https://onlinelibrary.wiley.com/terms-and-conditions) on Wiley Online Library for rules of use; OA articles are governed by the applicable Creative Commons License

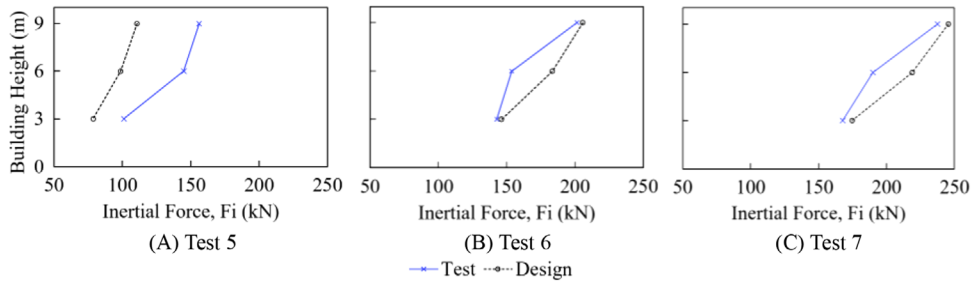


FIGURE 14 Peak story force versus diaphragm force in tests 5, 6 and 7 (phase 1).

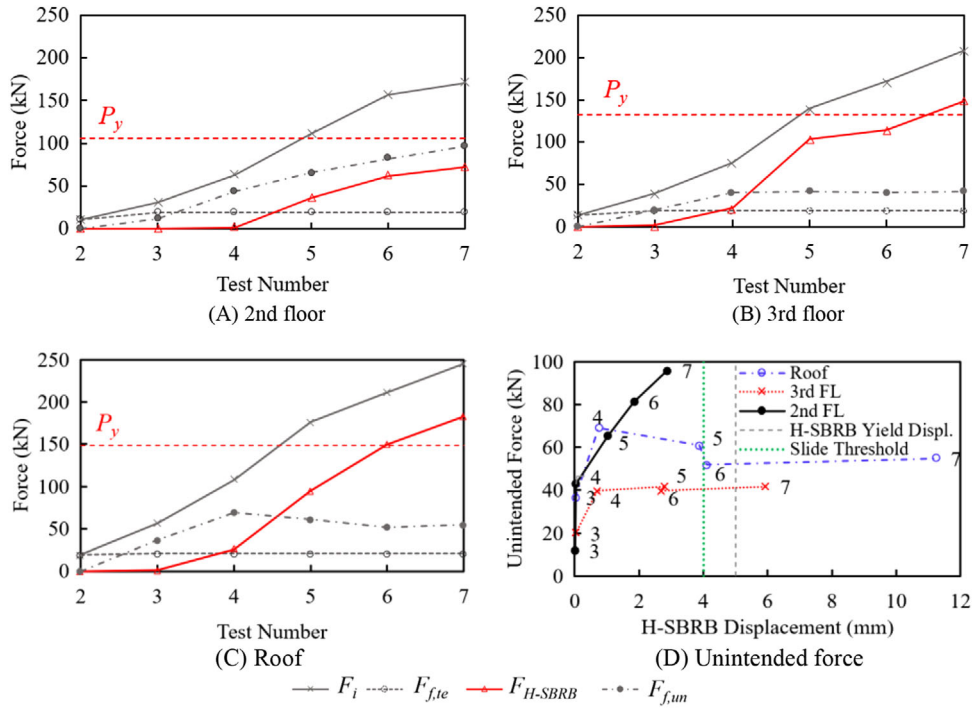


FIGURE 15 Composition of inertia force.

prevent the unintended torsion of the slab in tests. In test 6, the unintended force at the second floor was 52% of the inertial force (Figure 15A), limiting the H-SBRB force to reach only $0.6P_y$, where P_y is the actual yield force. On the third floor and roof, these forces were 23%−25% of the respective inertial forces so that the H-SBRB developed $0.86P_y$ and P_y, respectively. These unintended forces on the third floor and roof remained constant after test 5 as shown in Figure 15B and C. This indicates that the unintended force limited the H-SBRB from reaching the design force, particularly for the second floor. In general, as the slab sliding increased, the unintended force tended to increase and then remained constant after certain movement. However, the unintended force on the second floor kept on increasing because the slab movement was small compared to that of the upper two floors, as shown in Figure 15D, in which the number along a line represents the test number in phase 1. Therefore, 4 mm movement of the slab might be a threshold value, beyond which the unintended force approached constant in the test as seen from the response on the roof and third floor.

In general, the roof in phase 1 tests exhibited the largest slab sliding (Figure 9) and acceleration reduction among all floors because of H-SBRB yielding. In test 10 (phase 2), the slab relative displacement at the roof reached 12 mm as shown in Figure 10B, similar to that of test 7 in phase 1, so that a significant floor acceleration reduction is observed in Figure 12C. Since the H-SBRB was not used in phase 2 tests (i.e., all structural tee members remained elastic throughout the tests), the acceleration reduction is attributed to the unintended friction.

10969945, 2024, 9, Downloaded from https://onlinelibrary.wiley.com/doi/10.1002/eqe.4130 by Georgios Tsampras - University Of California , Wiley Online Library on [07/11/2026]. See the Terms and Conditions (https://onlinelibrary.wiley.com/terms-and-conditions) on Wiley Online Library for rules of use; OA articles are governed by the applicable Creative Commons License



(A) Beam in SMF (north end) (B) Beam in BRBF (north end)

FIGURE 16 Second floor beam end after test 10 (phase 2).



(A) First-story column top (B) Second-story column top (C) Third-story column top

(D) Column base (E) Second-story column bottom (F) Third-story column bottom

FIGURE 17 Center column after test 10 (phase 2).

6 | MODERATELY DUCTILE BOX COLUMN RESPONSE

In phase 2, the H-SBRB at each floor was replaced by a structural tee member to simulate a nearly rigid connection between the slab and beam so that moderately ductile box columns in a conventional dual system can be examined. No sign of column yielding was observed up to test 5 at the DBE level. Slight yielding as identified by whitewash flaking was observed at the bottom and top ends of the first-story CC as well as the second and third floor beam flanges in the SMF in test 6 (1.2 × MCE level). From tests 7 to 10, yielding in the CC ends propagated at three floors; no yielding was observed in the NC and SC. Significant yielding was also observed in the second and third floor beams within the RBS region, gusset plates, and the beam outside the gusset connection (Figure 16). Since the beams in the SMF acted as collectors for the inertial force at each floor, the beam in the roof reached a peak axial force of $0.12P_y$ in test 7 and $0.22P_y$ in test 8. No sign of local buckling was observed in the beams, gusset plates, or SBRBs after test 10 (Figure 16). Figure 17 shows the observation

10969945, 2024, 9, Downloaded from https://onlinelibrary.wiley.com/doi/10.1002/eqe.4130 by Georgios Tsampras - University Of California , Wiley Online Library on [07/11/2026]. See the Terms and Conditions (https://onlinelibrary.wiley.com/terms-and-conditions) on Wiley Online Library for rules of use; OA articles are governed by the applicable Creative Commons License

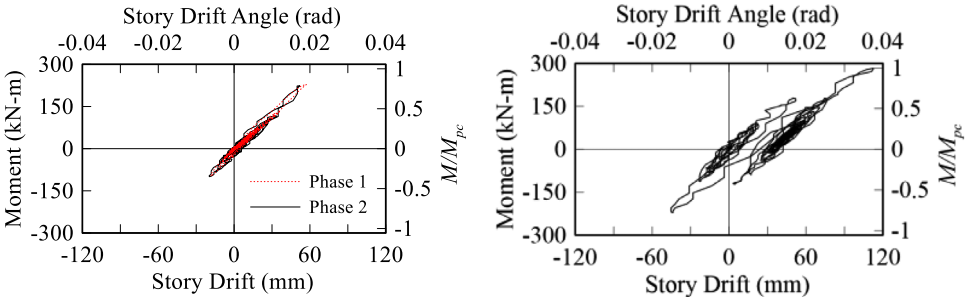


FIGURE 18 Base moment versus story drift of the first-story center column.

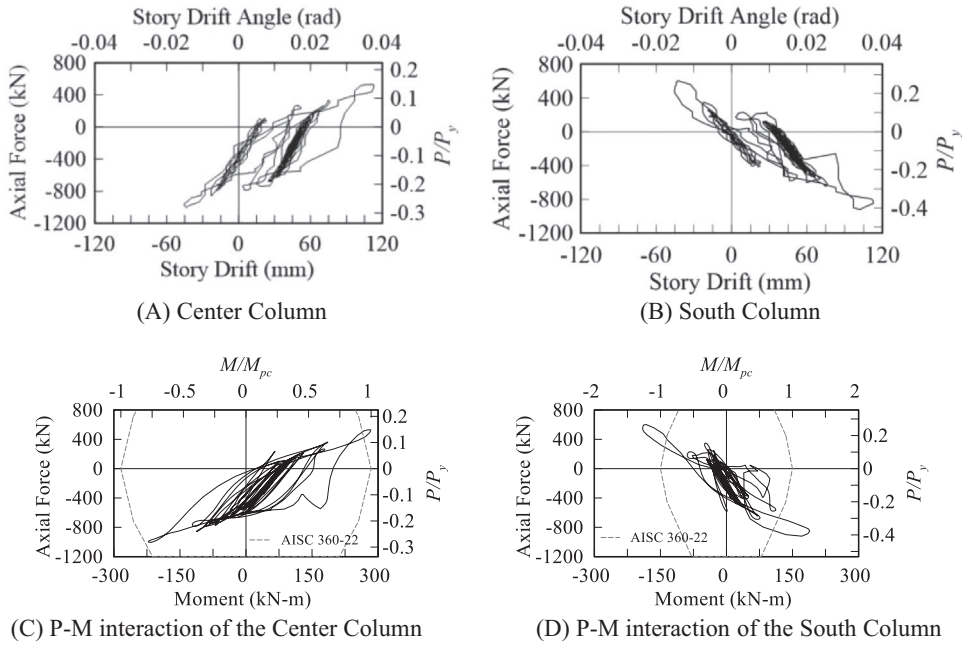


FIGURE 19 Axial force and P-M interaction in the first-story center and south columns (test 10).

of the CC at the three floors after test 10; significant yielding but with no sign of local buckling was observed at the column base. However, yielding was also observed at the top end of the third-story column.

Figure 18A shows the moment versus interstory drift at the base of the CC for test 7, where the axial compression force reached $0.22P_y$. In test 10, the CC showed a tensile force in the positive loading direction (Figure 19A) due to the overturning of the frame and the axial compression force induced by D-SBRBs. The D-SBRBs in the upper two stories also imposed considerable axial forces to the SC due to the brace arrangement (Figure 1B). The CC moment exceeded the plastic moment M_{pc} in tests 9 and 10 (Figure 18B), which caused the column to move from −0.018 to 0.38 rad with a residual drift angle of 0.012 rad. On the other hand, the axial compression of the SC increased from $0.03P_y$ to $0.41P_y$ (Figure 19B). Figure 19C and D show the P-M interaction for the first-story center and SCs in test 10. The CC response just reached the P-M yield surface computed based on AISC 360-22,[36] while the SC response exceeded the yield surface by about 25%−30%, probably due to strain hardening. The earthquake intensity that represents a seismic event of 2.4 × MCE resulted in a first-story interstory drift angle of 0.038 rad and a second-story drift angle of 0.045 rad. The built-up box columns performed well without strength degradation, although they only met the requirement for moderately ductile box column members in AISC 341-22.[1] The observed behavior indicates that λ_{hd} (= 12.2) for the highly ductile member requirement (Equation 1) in AISC 341-22[1] is too stringent because the columns in the frame specimen with b/t ratios of 20.5 and 21.1, close to λ_{md} (=22.2) of the moderately ductile column requirement (Equation 2), performed well in test 10. Since the I-shaped columns were pinned at the base, the column reamined elastic with much lower moment demands (i.e., a maximum value of 10% moment capacity = 15 kN-m) compared to the box column response (Figure 18B) in test 10.

10969945, 2024, 9, Downloaded from https://onlinelibrary.wiley.com/doi/10.1002/eqe.4130 by Georgios Tsampras - University Of California , Wiley Online Library on [07/11/2026]. See the Terms and Conditions (https://onlinelibrary.wiley.com/terms-and-conditions) on Wiley Online Library for rules of use; OA articles are governed by the applicable Creative Commons License

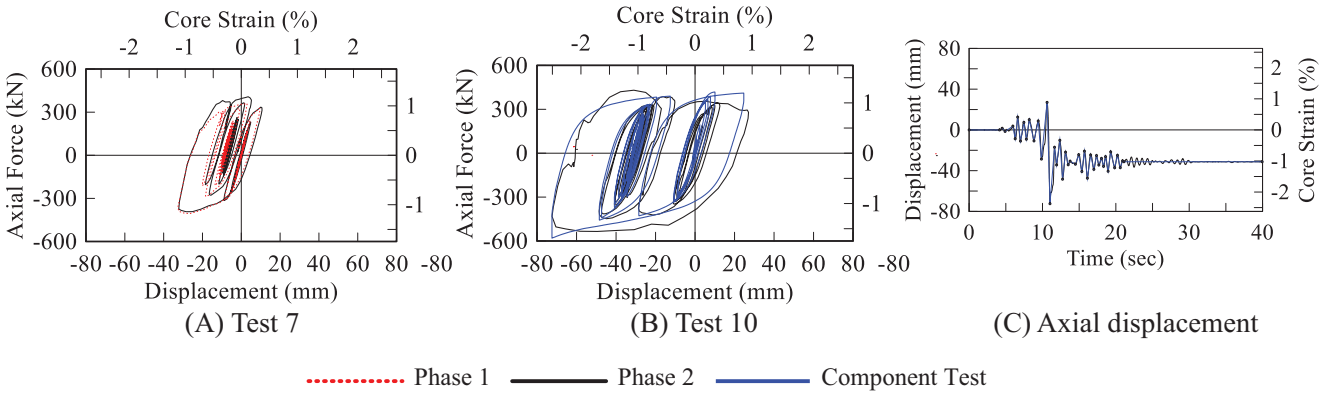


FIGURE 20 First-story D-sandwiched buckling-restrained brace (SBRB) response.

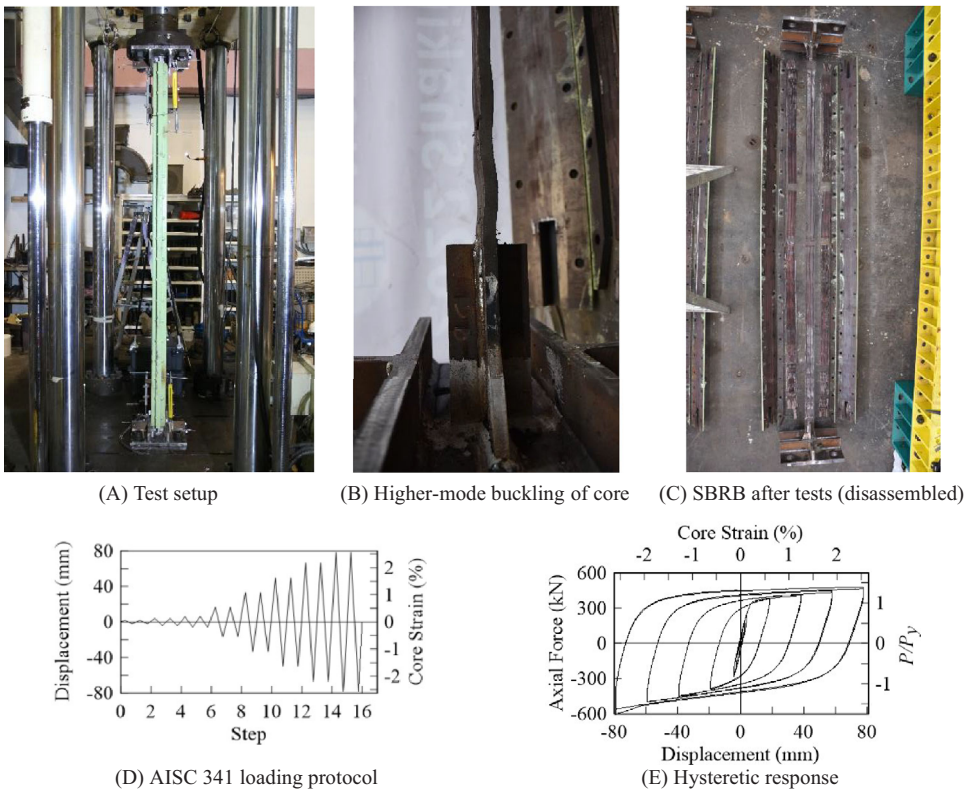


FIGURE 21 All-steel D-sandwiched buckling-restrained brace (SBRB) component tests.

7 | D-SBRB RESPONSE

The first-story D-SBRB yielded in test 5 with a maximum core strain of 0.4%, exceeding the yield strain of 0.2%. The axial core strain increased to 1.1% in test 7, where the brace response in phases 1 and 2 was similar (Figure 20A). The axial core strain increased to 2.5% in test 10 of phase 2 (Figure 20B). The maximum ductility ratio was 13 for the first-story brace, 13 for the second-story brace, and 10 for the third-story brace. The cumulative plastic ductility (CPD) was 217 for D-SBRB in the first story, 176 in the second story, and 112 in the third story for all 17 shaking table tests. The test results verify the satisfactory performance of all-steel SBRBs under a strong shaking with a velocity pulse moving to one direction with a maximum interstory drift angle of 0.045 rad.

After all shaking table tests, the first-story D-SBRB was removed from the frame specimen for retesting with a 5000 kN axial testing machine (Figure 21A). Two tests were conducted on the D-SBRB. First, the D-SBRB was tested by using the measured displacement history of the SBRB in test 10 (Figure 20C). The hysteretic response of the D-SBRB component test

10969845, 2024, 9, Downloaded from https://onlinelibrary.wiley.com/doi/10.1002/eqe.4130 by Georgios Tsampras - University Of California , Wiley Online Library on [07/11/2026]. See the Terms and Conditions (https://onlinelibrary.wiley.com/terms-and-conditions) on Wiley Online Library for rules of use; OA articles are governed by the applicable Creative Commons License

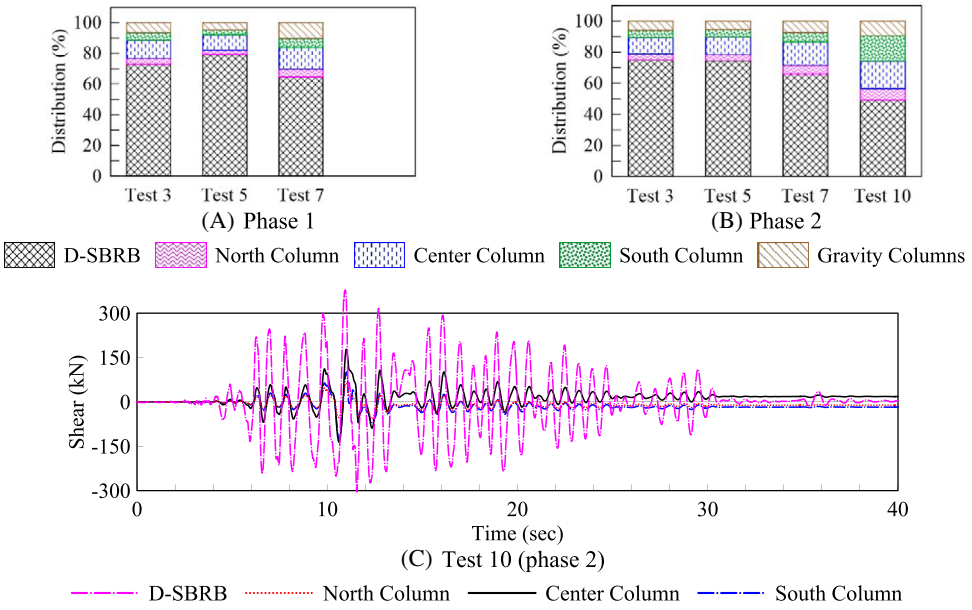


FIGURE 22 Base shear distribution.

was close to that obtained from the shaking table test, as shown in Figure 20B. Since the brace axial force in the shake table test was computed by subtracting the column shears (obtained from strain gauge data) from the story shears (obtained from accelerometer data), similar responses in Figure 20B validate the data processing for the story shear and column moment in the shake table tests. The second phase of the component test was performed using the AISC 341-22[1] loading protocol (Figure 21D), and its response is shown in Figure 21E. Figure 21B and C show higher-mode buckling of the core plate after removing bolts from the restraining members of the SBRB. The higher-mode buckling in the core plate started from the end of stiffeners of the SBRB (Figure 21B) and extended 250 mm toward the core plate center; no higher-mode buckling was observed in the center portion of the core plate. A scratch mark was found at the ends of the restrained member, which may have been the cause for the force increase near 2.5% strain in the last cycle, as shown in Figure 21E. No global buckling or fracture was found in the restraining member or core plate after brace component tests. The total CPD of the D-SBRB increased to 526 from 217 after all tests.

Figure 22A and B show the base shear distribution in phase 1 and 2 tests. From tests 3 to 5 in phase 1, the story shear carried by D-SBRBs increased from 73% to 79%, but decreased to 65% in test 7 due to significant yielding in SBRBs when compared to the nearly elastic response of box columns. Although the gravity frame used a simple framing at the beam-to-column connections and the column bases (Figure 1E), 6%–10% base shear was still resisted by these columns. Similar force distribution between D-SBRBs and columns can be found in phase 2. A significant force reduction of the D-SBRBs to 49% can be found in test 10, indicating that when the D-SBRB is in a fully yield level its story shear carrying capacity is reduced compared to the box column. Figure 22C shows the shear distribution history at the first story in test 10, indicating that the CC carried about two times the shear in the north and SCs.

8 | CONCLUSIONS

The highly ductile requirement [λ_{hd} in Equation 1] for the built-up box column in AISC 341[1,2] is conservative when comparing the hysteretic responses of isolated highly ductile box columns and I-shaped columns under the same loading condition.[4] This research aimed to evaluate the seismic performance of built-up box columns in a full-scale, 3-story steel dual frame system with a BRBF and a backup SMF through shaking table tests. The built-up box columns used for the frame specimen had a width-to-thickness ratio of 20–21, which met only the moderately ductile column requirement ($\lambda_{md} = 22.2$) in AISC 341-22.[1] The frame specimen was tested using a shake table at the NCREE Tainan laboratory. In addition to investigating the column compactness requirement, the other objective was to study the building response by using a sliding slab concept. Therefore, two test phases were conducted on the building specimen: (1) slabs designed to slide relative to the LFRS in phase 1, and (2) slabs rigidly connected to the LFRS to simulate the conventional frame in phase 2. Main findings from this research are summarized below.

10969945, 2024, 9, Downloaded from https://onlinelibrary.wiley.com/doi/10.1002/eqe.4130 by Georgios Tsampras - University Of California , Wiley Online Library on [07/11/2026]. See the Terms and Conditions (https://onlinelibrary.wiley.com/terms-and-conditions) on Wiley Online Library for rules of use; OA articles are governed by the applicable Creative Commons License

1. For the 3-story building tested, the slab on the roof had a larger lateral displacement than other floors. In phase 1 testing, the slab started to slide in test 4 with PGA = 0.17 g, and showed a significant displacement relative to the LFRS in test 5 (DBE level), as shown in Figure 10B. The H-SBRB in the roof showed yielding, resulting in a floor acceleration reduction of 25% when compared to that in phase 2 testing (Figure 12C). Additionally, the story shear in phase 1 was found to be lower than that in phase 2, particularly in test 7. Although Teflon pads were used between the slabs and the beams, the unintended friction force, which resulted from beams moving against lateral bracings and slabs moving against guide plates, limited slab sliding. Despite the unexpected friction force, the H-SBRB was still effective to transfer the initial force from the slab to the LFRS and reduced the floor acceleration through its energy dissipation capacity.
2. In test 10 (phase 2), the maximum base shear was about 3.2 times the design base shear. The maximum interstory drifts were 0.038 rad at the second floor, 0.045 rad at the third floor, and 0.031 rad at the roof (Figure 7B). The CC developed the plastic moment M_{pc} when the column moved from −0.018 to 0.038 rad with a residual drift angle of 0.012 rad. The SC also reached M_{pc} with a maximum column axial force of $0.41P_y$ (Figure 19B). No local buckling was observed near the base of all columns in the frame specimen. The test results indicate that the b/t requirement for highly ductile built-up box columns in AISC 341-22[1] is overly conservative. Columns used in the frame specimen with a large b/t value (e.g., 21) that significantly exceeded the highly ductile column requirement ($\lambda_{hd} = 12.2$) in AISC 341-22[1] still provided satisfactory performance of the first-story columns at large drifts (i.e., 0.038 rad).
3. The strain of the core in the first-story all-steel D-SBRB reached 2.5%; its CPD was 217 after all shake table tests with very stable response (Figure 20B). The hysteretic responses of the D-SBRB from the shake table test and the postearthquake single component test were similar, verifying the data processing and the associated lateral force distribution in the LFRS. The all-steel D-SBRB was disassembled by removing bolts from the restraining members; a scratch mark was found near both ends of the restraining member due to the higher-mode buckling in the core plate ends, which may have been the cause for the force increase in the last cycle of the brace test (see Figure 21E).

Further research is needed on the testing of the multistory sliding floor system with different LFRS to assess the effect of story stiffness on the floor sliding response. Multidirectional shaking is also needed to address potential challenges for practical implementation.

ACKNOWLEDGMENTS

This work was funded by the National Science and Technology Council under the project number MOST 111-2625-M-002-006, Taiwan and the 2022 Innovative Project of National Applied Research Laboratories.

DATA AVAILABILITY STATEMENT

The data that support the findings of this study are available from the corresponding author upon reasonable request.

ORCID

Chung-Che Chou https://orcid.org/0000-0002-6791-3790
Chin-Hsiung Loh https://orcid.org/0000-0003-1007-5041
Hsuan-Teh Hu https://orcid.org/0000-0001-8582-0670

REFERENCES

1. AISC. *Seismic Provisions for Structural Steel Buildings*. ANSI/AISC 341-22. American Institute of Steel Construction; 2022.
2. AISC. *Seismic Provisions for Structural Steel Buildings*. ANSI/AISC 341-16. American Institute of Steel Construction; 2016.
3. Chou CC, Chen GW. Lateral cyclic testing and backbone curve development of high-strength steel built-up box columns under axial compression. *Eng Struct*. 2020;223:111147.
4. Lin TH, Chou CC. High-strength steel deep H-shaped and box columns under proposed near-fault and post-earthquake loadings. *Thin Walled Struct*. 2022;172:108892.
5. Lignos DG, Krawinkler H. A steel database for component deterioration of tubular hollow square steel columns under varying axial load for collapse assessment of steel structures under earthquakes. Paper presented at: Proceedings of the 7th International Conference on Urban Earthquake Engineering (7CUEE); 2010.
6. Suzuki Y, Lignos DG. Experimental evaluation of steel columns under seismic hazard-consistent collapse loading protocols. *J Struct Eng*. 2021;147(4):04021020.
7. Elkady A, Lignos DG. Full-scale testing of deep wide-flange steel columns under multiaxis cyclic loading: loading sequence, boundary effects, and lateral stability bracing force demands. *J Struct Eng*. 2018;144(2):04017189. ASCE.
8. Chansuk P, Ozkula G, Uang CM, Harris JL. Seismic behavior and design of deep, slender wide-flange structural steel beam-columns. In: *Technical Note 2169*. National Institute of Standards and Technology; 2021.

10969845, 2024, 9, Downloaded from https://onlinelibrary.wiley.com/doi/10.1002/eqe.4130 by Georgios Tsampras - University Of California , Wiley Online Library on [07/11/2026]. See the Terms and Conditions (https://onlinelibrary.wiley.com/terms-and-conditions) on Wiley Online Library for rules of use; OA articles are governed by the applicable Creative Commons License

9. Chou CC, Lai YC, Xiong HC, et al. Effect of boundary condition on the cyclic response of I-shaped steel columns: two-story subassemblage versus isolated column tests. *Earthq Eng Struct Dyn*. 2022;51:3434-3455. doi:10.1002/eqe.3730
10. Chou CC, Xiong HC, Kumar A, Lai YC, Uang CM. Effects of section compactness and SCWB condition on moment redistribution and plastic hinging in SMF built-up box columns. *J Struct Eng*. 2023;149(11):04023144.
11. Wang KJ, Chou CC, Huang CW, et al. Hybrid simulation of a steel dual system with buckling-induced first-story column shortening: a mixed control mode approach. *Earthq Eng Struct Dyn*. 2023;52:3727-3745. doi:10.1002/eqe.3944
12. Suita K, Yamada S, Tada M, Kasai K, Matsuoka Y, Sato E, Results of recent E-Defense tests on full-scale steel buildings: part 1—collapse experiments on 4-story moment frames. Paper presented at: Structures Congress 2008: Crossing Borders; 2008:1-10.
13. Lignos DG, Hikino T, Matsuoka Y, Nakashima M. Collapse assessment of steel moment frames based on E-Defense full-scale shake table collapse tests. *J Struct Eng*. 2013;139(1):120-132.
14. Mar D, Tipping S. Story isolation: a new high-performance seismic technology. Paper presented at: *9th US-Japan Workshop on the Improvement of Structural Design and Construction Practices; 2000; Victoria*.
15. Villaverde R. Roof isolation system to reduce the seismic response of buildings: a preliminary assessment. *Earthq Spectra*. 1998;14(3):521-532.
16. Villaverde R. Aseismic roof isolation system: feasibility study with 13-story building. *J Struct Eng*. 2002;128(2):188-196.
17. Villaverde R, Aguirre M, Hamilton C. Aseismic roof isolation system built with steel oval elements: exploratory study. *Earthq Spectra*. 2005;21(1):225-241.
18. Cui S, Bruneau M, Kasalanati A. Behavior of bidirectional spring unit in isolated floor systems. *J Struct Eng*. 2010;136(8):944-952.
19. Cui S, Bruneau M, Kasalanati A. Seismic response case study of isolated floor system having special biaxial spring units. *J Struct Eng*. 2016;142(12):05016002.
20. Liu S, Warn GP. Seismic performance and sensitivity of floor isolation systems in steel plate shear wall structures. *Eng Struct*. 2012;42:115-126.
21. Anajafi H, Medina RA. Robust design of a multi-floor isolation system. *Struct Control Health Monit*. 2018;25(4):e2130.
22. Casagrande L, Villa E, Nespoli A, Occhiuzzi A, Bonati A, Auricchio F. Innovative dampers as floor isolation systems for seismically-retrofit multi-storey critical facilities. *Eng Struct*. 2019;201:109772.
23. Xiang Y, Koetaka Y. Structural feasibility of incorporating the LVEM-isolated floor in the first story of a two-story steel frame. *Eng Struct*. 2019;199:109686.
24. Xiang Y, Koetaka Y, Nishira K. Steel frame with aseismic floor: from the viscoelastic decoupler model to the elastic structural response. *Earthq Eng Struct Dyn*. 2021;50(6):1651-1670.
25. Lin HZ. Shake Table Tests of a Full-Scale Three-Story Steel Dual Frame under the 2022 Chishang Earthquake: Seismic Performance of Moderately Ductile Box Column, All-Steel Sandwiched Buckling-Restrained Brace, and Sliding Slab. Thesis. Department of Civil Engineering, National Taiwan University; 2023. (In Chinese).
26. Taiwan Code. *Design and Technique Specifications of Steel Structures for Buildings*. Construction and Planning Agency, Ministry of the Interior; 2010.
27. AISC. *Prequalified Connections for Special and Intermediate Steel Moment Frames for Seismic Applications*. AISC 358-16. AISC; 2016.
28. Chou CC, Chen SY. Subassemblage tests and finite element analyses of sandwiched buckling-restrained braces. *Eng Struct*. 2010;32:2108-2121.
29. Chou CC, Liu JH, Pham DH. Steel buckling-restrained braced frames with single and dual corner gusset connections: seismic tests and analyses. *Earthq Eng Struct Dyn*. 2012;41(41):1137-1156.
30. Pham DH, Chou CC. Strong-axis instability of sandwiched buckling restrained braces in a steel two-story X-BRBF: seismic tests and finite element analyses. *Thin Walled Struct*. 2020;157:107011.
31. Lin BZ, Chuang MC, Tsai KC. Object-oriented development and application of a nonlinear structural analysis framework. *Adv Eng Softw*. 2009;40(1):66-82.
32. ASCE/SEI 7-22. *Minimum Design Loads and Associated Criteria for Buildings and Other Structures*. American Society of Civil Engineers; 2022.
33. Chou CC, Wu CL, Chai JF, Yao GC. Reconnaissance Report on Seismic Damage Caused by the 2022 Guanshan and Chihshang Earthquake Sequence, Taiwan. Rept. No. NCREE-23-007. National Center for Research on Earthquake Engineering; 2023.
34. Iwan WD, Moser MA, Peng CY. Some observations on strong-motion earthquake measurement using a digital accelerograph. *Bull Seismol Soc Am*. 1985;75:1225-1246.
35. Chen JM. One-Story Steel Frame Tests Using a Stiffness Adjustable Self-Centering Brace and Sandwiched Buckling-Restrained Brace. Thesis. Department of Civil Engineering, National Taiwan University; 2023. (In Chinese).
36. AISC. *Specification for Structural Steel Buildings*. ANSI/AISC 360-22. American Institute of Steel Construction; 2022.

How to cite this article: Chou C-C, Lin H-Z, Córdova A, et al. Earthquake simulator testing of a three-story steel building for evaluating built-up box column performance and effect of sliding slab. *Earthquake Engng Struct Dyn*. 2024;53:2637–2655. https://doi.org/10.1002/eqe.4130

10969845, 2024, 9, Downloaded from https://onlinelibrary.wiley.com/doi/10.1002/eqe.4130 by Georgios Tsampras - University Of California , Wiley Online Library on [07/11/2026]. See the Terms and Conditions (https://onlinelibrary.wiley.com/terms-and-conditions) on Wiley Online Library for rules of use; OA articles are governed by the applicable Creative Commons License